The Alzheimer Structural Connectome: Changes in Cortical Network Topology with Increased Amyloid Plaque Burden[1]

Jeffrey W. Prescott, MD, PhD
Arnaud Guidon, PhD
P. Murali Doraiswamy, MBBS, FRCP
Kingshuk Roy Choudhury, PhD
Chunlei Liu, PhD
Jeffrey R. Petrella, MD
For the Alzheimer's Disease Neuroimaging Initiative

Purpose: To evaluate differences in the structural connectome among patients with normal cognition (NC), mild cognitive impairment (MCI), and Alzheimer disease (AD) and to determine associations between the structural connectome and cortical amyloid deposition.

Materials and Methods: Patients enrolled in a multicenter biomarker study (Alzheimer's Disease Neuroimaging Initiative [ADNI] 2) who had both baseline diffusion-tensor (DT) and florbetapir positron emission tomography (PET) data at the time of data analyses in November 2012 were studied. All institutions received institutional review board approval. There were 102 patients in ADNI 2 who met criteria for analysis. Patients' T1-weighted images were automatically parcellated into cortical regions of interest. Standardized uptake value ratio (SUVr) was calculated from florbetapir PET images for composite cortical regions (frontal, cingulate, parietal, and temporal). Structural connectome graphs were created from DT images, and connectome topology was analyzed in each region by using graph theoretical metrics. Analysis of variance of structural connectome metrics and florbetapir SUVr across diagnostic group was performed. Linear mixed-effects models were fit to analyze the effect of florbetapir SUVr on structural connectome metrics.

Results: Diagnostic group (NC, MCI, or AD) was associated with changes in weighted structural connectome metrics, with decreases from the NC group to the MCI group to the AD group shown for *(a)* strength in the bilateral frontal, right parietal, and bilateral temporal regions ($P < .05$); *(b)* weighted local efficiency in the left temporal region ($P < .05$); and *(c)* weighted clustering coefficient in the bilateral frontal and left temporal regions ($P < .05$). Increased cortical florbetapir SUVr was associated with decreases in weighted structural connectome metrics; namely, strength ($P = .00001$), weighted local efficiency ($P = .00001$), and weighted clustering coefficient ($P = .0006$), independent of brain region. For every 0.1-unit increase in florbetapir SUVr, there was a 14% decrease in strength, an 11% decrease in weighted local efficiency, and a 9% decrease in weighted clustering coefficient, regardless of the analyzed cortical region or, in the case of weighted local efficiency and clustering coefficient, diagnostic group.

Conclusion: Increased amyloid burden, as measured with florbetapir PET imaging, is related to changes in the topology of the large-scale cortical network architecture of the brain, as measured with graph theoretical metrics of DTI tractography, even in the preclinical stages of AD.

Online supplemental material is available for this article.

[1] From the Department of Radiology (J.W.P., K.R.C., J.R.P.), Department of Psychiatry (P.M.D.), Department of Medicine (P.M.D.), and Duke Institute for Brain Sciences (P.M.D.), Duke University Medical Center, Box 3808, Durham, NC 27710; and Brain Image Analysis Center, Duke University, Durham, NC (A.G., C.L.). Received November 8, 2013; revision requested December 26; revision received March 11, 2014; accepted March 17; final version accepted March 21. **Address correspondence to** J.W.P. (e-mail: *jeffrey.prescott@duke.edu*).

Alzheimer disease (AD) is a progressive neurodegenerative dementia that affects approximately 5.5 million people in the United States and about 30 million people worldwide. It is believed to have a prolonged prodromal and preclinical phase initially characterized by the development of silent pathologic changes (preclinical AD) and followed by mild cognitive impairment (MCI) and then dementia (1). β-Amyloid plaques and neurofibrillary tangles are pathologic hallmarks of AD, and there is great interest in elucidating how these core disorders relate to changes in brain structure and function, and in turn, how they relate to deficits in cognition (2). There is growing evidence that the cognitive deficits in patients with AD can be understood in terms of abnormal interactions or connections among brain regions better than they can be understood by deficits in any one brain region (3). Thus, the study of how functional and structural brain networks are altered by AD might provide a critical link between our understanding of AD neuropathology and its cognitive manifestations. The advent of new imaging technologies with which to depict in vivo amyloid plaques and large-scale functional and structural brain networks is beginning to shed light on this critical question.

β-Amyloid positron emission tomography (PET) enables noninvasive assessment of the amyloid burden. Florbetapir is a fluorine 18–labeled radioligand that recently was approved by the Food and Drug Administration for use in the assessment of β-amyloid plaques in the setting of progressive cognitive decline. Quantitative and qualitative measures of cortical florbetapir uptake have correlated with postmortem β-amyloid burden and with longitudinal cognitive decline (4,5).

The term *connectomics* refers to mapping of the neural connections and networks in the brain, including structural and functional networks (6,7). The large-scale functional and structural networks of the brain can be mapped and analyzed by applying graph theoretical analyses to functional magnetic resonance (MR) imaging time series data for functional networks and diffusion-tensor imaging tractography data for structural networks. Specifically, by using the term *node* to define a particular cortical region of interest in a graph and by using interregion time series correlations or tractography streamlines as edges, quantitative analysis of the organization or topology of the connectome can be performed (7,8).

Initial connectomics studies in patients with AD focused on the functional connectome (9–13). These works have shown that time-dependent interactions between brain regions are altered as AD progresses, both with clinical signs and symptoms and with pathologic changes, such as increased β-amyloid plaque formation. Previous tractographic studies have shown decreased network complexity in patients with MCI or AD as compared with healthy control patients, with differences in connectivity located predominantly in the frontal regions (14–17). To our knowledge, no prior study has been performed to examine the relationship between amyloid plaque disease and structural connectivity. The purpose of our study was to evaluate differences in the structural connectome between patients with normal cognition (NC), patients with MCI, and patients with AD and to examine how structural connectivity might change with increased cortical amyloid deposition.

Advances in Knowledge

- Increased cortical amyloid burden is associated with changes in the topology of the structural connectome, as measured with graph theoretical metrics; namely, there are significant decreases in strength ($P = .00001$), weighted local efficiency ($P = .00001$), and weighted clustering coefficient ($P = .0006$) that are similar across all analyzed brain regions.
- The degree of amyloid burden is more strongly associated with changes in the structural connectome than with diagnostic group (normal cognition, mild cognitive impairment, or Alzheimer disease [AD]).
- For every 0.1-unit increase in florbetapir standardized uptake value ratio, there was a 14% decrease in strength, an 11% decrease in weighted local efficiency, and a 9% decrease in weighted clustering coefficient; thus, large-scale structural network changes can be detected in the presence of amyloid pathology, even in the preclinical stages of AD.

Implication for Patient Care

- These results suggest that structural network changes need to be a target for therapy early in the course of AD.

Materials and Methods

We studied patients enrolled in a multicenter biomarker study, the Alzheimer's Disease Neuroimaging Initiative (ADNI) 2, who had both DT imaging and florbetapir PET data at the start of data analyses in November 2012. Analyses

Published online before print
10.1148/radiol.14132593 **Content code:** NR

Radiology 2014; 273:175–184

Abbreviations:
AD = Alzheimer disease
ADNI = Alzheimer's Disease Neuroimaging Initiative
DT = diffusion tensor
MCI = mild cognitive impairment
NC = normal cognition
SUVr = standardized uptake value ratio

Author contributions:
Guarantors of integrity of entire study, J.W.P., J.R.P.; study concepts/study design or data acquisition or data analysis/interpretation, all authors; manuscript drafting or manuscript revision for important intellectual content, all authors; approval of final version of submitted manuscript, all authors; literature research, J.W.P., A.G., J.R.P.; clinical studies, J.W.P., A.G., P.M.D., J.R.P.; statistical analysis, J.W.P., A.G., K.R.C.; and manuscript editing, J.W.P., A.G., P.M.D., C.L., J.R.P.

Funding:
This research was supported by the National Institutes of Health (grants U01 AG024904, P30 AG010129, K01 AG030514, and R01 MH096979).

Conflicts of interest are listed at the end of this article.

Table 1

Patient Characteristics across Diagnostic Groups

Characteristic	NC Group ($n = 37$)	MCI Group ($n = 44$)	AD Group ($n = 21$)	*P* Value
Age (y)	73.8 ± 6.1 7	1.8 ± 12.8	75.0 ± 9.8	.66
Sex*				.36
Male	20 (54)	29 (66)	15 (71)	…
Female	17 (46)	15 (34)	6 (29)	…
Education (y)	16.5 ± 2.7	15.3 ± 2.9	15.3 ± 3.2	.17
ADAS-cog	5.3 ± 2.9	11.1 ± 4.6	20.5 ± 7.2	<.001

Note.—Unless otherwise indicated, data are mean ± standard deviation. *P* values are from analysis of variance of characteristic versus diagnostic group. ADAS-cog = Alzheimer's Disease Assessment Scale-cognitive subscale.

* Data are number of patients, with percentages in parentheses.

were performed from November 2012 to November 2013. ADNI 2 was conducted at more than 50 institutions in North America. Of these institutions, 15 acquired DT images and were included in this study. All institutions received institutional review board approval for study participation. Patients enrolled in ADNI 2 were aged 55 to 90 years and had no other clinically important neurologic condition. Although 550 patients were studied in ADNI 2, only a subset of those who underwent both DT imaging and florbetapir PET met the criteria for inclusion in this analysis (Table 1). Patients included in this study were enrolled between April 2011 and August 2012. There are four clinical diagnostic arms in ADNI 2: patients with NC, patients with early MCI, patients with late MCI, and patients with AD. For the purpose of this study, patients with early MCI and those with late MCI were combined into one MCI group; patients with early MCI and those with late MCI had a Mini-Mental State Examination score of 24–30 and a Clinical Dementia Rating of 0.5 (18). Each patient underwent baseline cognitive assessment, T1-weighted MR imaging, DT imaging, and florbetapir PET imaging. The ADNI 2 protocol describes the acquisition methods in depth *(www.adni-info.org)*. All data were anonymized and centrally housed by ADNI. In general, the anatomic T1-weighted spoiled gradient-recalled images and DT images were acquired during the same session with one of two MR imagers (Signa HDxt or Discovery MR 750; GE Medical Systems, Milwaukee, Wis). Most florbetapir PET images were acquired within 3 months of the T1-weighted and DT images, with a maximum of 8 months between acquisitions. Analysis of variance revealed no significant differences in time between examinations among the diagnostic groups ($P = .86$).

All image processing and analyses were performed by two authors (J.W.P., A.G.; each with 10 years of experience).

Anatomic T1-weighted MR Image Acquisition and Processing

Anatomic 3-T T1-weighted MR images were acquired. Because DT images were acquired only with the aforementioned imagers in the ADNI 2 study, the T1-weighted sequence used was that of the aforementioned imagers, namely the spoiled gradient-recalled sequence.

The T1-weighted images were segmented by using the FreeSurfer (version 5.1.0; *surfer.nmr.mgh.harvard.edu*) default automated gyral-based parcellation method, and this yielded 83 cortical and subcortical regions of interest (19,20).

Florbetapir (Amyloid) PET Image Acquisition and Processing

PET image acquisition was performed 50–70 minutes after injection of 10 mCi (370 MBq) of florbetapir. The acquired images were centrally processed by ADNI, including spatial alignment, averaging, interpolation to a standard voxel size, and smoothing by 8-mm full width at half maximum (described at *adni.loni.ucla.edu/methods/pet-analysis/preprocessing/*).

The FreeSurfer parcellations were automatically registered to the florbetapir PET images by using a transformation calculated with maximization of mutual information between the T1-weighted anatomic images and the florbetapir PET images. Four composite cortical regions were created in each cerebral hemisphere by combining regions from the FreeSurfer parcellation, as follows: *(a)* The lateral and medial frontal region (hereafter, frontal region) included the caudal middle frontal, lateral orbitofrontal, medial orbitofrontal, pars opercularis, pars orbitalis, pars triangularis, rostral middle frontal, superior frontal, and frontal pole regions. *(b)* The anterior and posterior cingulate region (hereafter, cingulate region) included the caudal anterior cingulate, isthmus cingulate, posterior cingulate, and rostral anterior cingulate regions. *(c)* The lateral parietal region (hereafter, parietal region) included the inferior parietal, precuneus, superior parietal, and supramarginal regions. *(d)* The lateral temporal region (hereafter, temporal region) included the middle temporal and superior temporal regions. These regions are based on prior analyses that showed high test-retest reliability for average cortical standardized uptake value ratio (SUVr) quantitative analysis of florbetapir PET in patients with AD (18,21). It should be noted that these regions did not include the inferior temporal cortex, entorhinal cortex, amygdalae, or hippocampi, all of which are areas known to be affected in patients with AD.

Next, weighted SUVr of the four composite cortical regions was determined by first calculating the volume-weighted average standardized uptake value (SUV) of the voxel values from the constituent FreeSurfer parcellations of each composite region with the following equation:

$$\overline{\mathrm{SUV}}_{\mathrm{region}} = \frac{\sum_{r\in\mathrm{region}}\sum_{i\in r} I(i)V(i)}{\sum_{r\in\mathrm{region}}\sum_{i\in r} V(i)}, \quad (1)$$

where *region* represents the frontal, cingulate, parietal, or temporal region; *r* represents a subregion of the current region; *I(i)* is the standardized uptake value of the voxel *i*; *V(i)* is the volume

of the voxel *i*. The SUVr of each region was calculated by dividing standardized uptake value of the region by the average standardized uptake value of the whole cerebellum ($\overline{\text{SUV}}_{\text{whole cerebellum}}$).

DT Image Acquisition

The DT images were acquired with the aforementioned MR imagers. Acquisition parameters were as follows: spin-echo echo-planar imaging sequence; *b* value, 1000 sec/mm^2; b0 = 0 (five signal averages), with 41 isotropically distributed diffusion-sensitizing gradients; and acquisition image size, 2.7 × 2.7 × 2.7 mm, with an applied reduction factor of two. For the Signa HDxt imager, repetition time was 12500 msec and echo time was 68 msec. For the Discovery MR 750 imager, repetition time was 9050 msec and echo time was 63 msec. All DT images were visually assessed for patient motion and distortion artifacts. No images were excluded from analysis because of excessive patient motion or distortion artifacts.

Structural Connectome Construction

Structural connectome graphs were constructed from the DT images by using the Connectome Mapping Toolkit (version 1.2.0; Ecole Polytechnique Fédérale de Lausanne and Hospital Center and University of Lausanne, Lausanne, Switzerland), with 32 random seeds per voxel, an angular threshold of 60°, and a step size of 0.5 mm (22). The B_0 images from the DT images were registered to the T1-weighted anatomic images by using the Functional Magnetic Resonance Imaging of the Brain linear image registration tool (FLIRT) with the maximization of mutual information method (23). The transformation from this registration was then used to register the FreeSurfer parcellation to the connectome graph. Each FreeSurfer cortical and subcortical gray matter region was set as a node, excluding the brain stem, for a total of 82 nodes (41 per hemisphere). This was done to assess the association between the florbetapir SUVr of a region and all of its tractographic connections, not only the connections between the analyzed florbetapir PET regions (frontal, cingulate, parietal, and temporal). Tractographic streamline volumes were visually assessed for patient motion and distortion artifacts. No images were excluded from analysis because of excessive patient motion or distortion artifacts.

Structural Connectome Graph Theoretical Analysis

The Brain Connectome Toolbox was used to calculate graph theoretical metrics for the connectome graphs (8). The metrics calculated included both unweighted (binary) and weighted (number of streamlines) forms. In general, binary networks are easier to characterize; however, there is loss of information on the strength of connections, which may prove critical in the precise characterization of network organization (8).

The unweighted metrics were calculated by setting an edge with a value of 1 if there was any connection between two nodes and setting an edge with a value of 0 if there was no connection. The weighted metrics were calculated by setting the edge weights as the number of streamlines connecting two nodes. The metrics calculated were degree (number of nodes connected to a node; unweighted), strength (number of streamlines connected to a node; weighted), local efficiency (average inverse shortest path length in a node neighborhood; both unweighted and weighted), and clustering coefficient (the fraction of a node's neighbors that are neighbors of each other; both unweighted and weighted).

Graph theoretical measures of network topology can be classified broadly into those that measure integration and those that measure segregation (7,8). Both local efficiency and clustering coefficient can be taken as measures of segregation, which quantify the presence of densely interconnected groups, or clusters, of brain regions. Structural networks have been shown to be both highly segregated and highly integrated, forming a so-called small-world network (24). High segregation is a marker for complexity in a network, and a decrease in segregation can be taken as a representation of change toward a more random topologic organization. In terms of the measures of segregation analyzed in this article, complex networks have a high local efficiency and clustering coefficient, while random networks have a low local efficiency and clustering coefficient (7).

In the case of calculation of weighted local efficiency, the number of streamlines were normalized to a range of 0–1 by dividing the number of streamlines between each node by the maximum number of streamlines between any two nodes in the graph. Subsequent statistical analysis was performed on only the 38 cortical regions (nodes) (19 per hemisphere) that were included in the composite regions, as described perviously (ie, frontal, cingulate, parietal, and temporal). For the regional structural connectome metrics, the metrics of the nodes in each composite region were averaged together without adjustment for volume to produce an average network metric value.

Statistical Analysis

Summary statistics were computed for demographics and clinical characteristics. Differences in regional structural connectome metrics and florbetapir SUVr were examined by using one-way analysis of variance across diagnostic group (NC, MCI, or AD). These analyses were exploratory and were not adjusted for multiple comparisons.

A linear mixed-effects model was used to analyze the relationship between regional florbetapir SUVr and the network metrics. The following model was used:

$$\begin{aligned}\ln(M_{ik}) = {} & \mu + a_i + \alpha_{\text{MCI},i} + \alpha_{\text{AD},i} \\ & + \alpha_{F,i} + \alpha_{Rk} + b_p \text{SUVr}_{\text{LF},i} \\ & + b_{p,\text{MCI}} \text{SUVr}_{\text{LF},i} \\ & + b_{p,\text{AD}} \text{SUVr}_{\text{LF},i} \\ & + b_{p,k} \text{SUVr}_{ik} + b_a \text{Age}_i \\ & + b_e \text{Educ}_i + \varepsilon_k . \end{aligned} \quad (2)$$

The outcome M_{ik} is the structural metric computed at region *k* for patient *i*. The model explains variation in this metric in terms of a baseline average μ, which represents the expected metric value in the left frontal region of a healthy 74-year-old man with 16 years of education. Thus, the baseline corresponds to a patient possessing average values

Figure 1

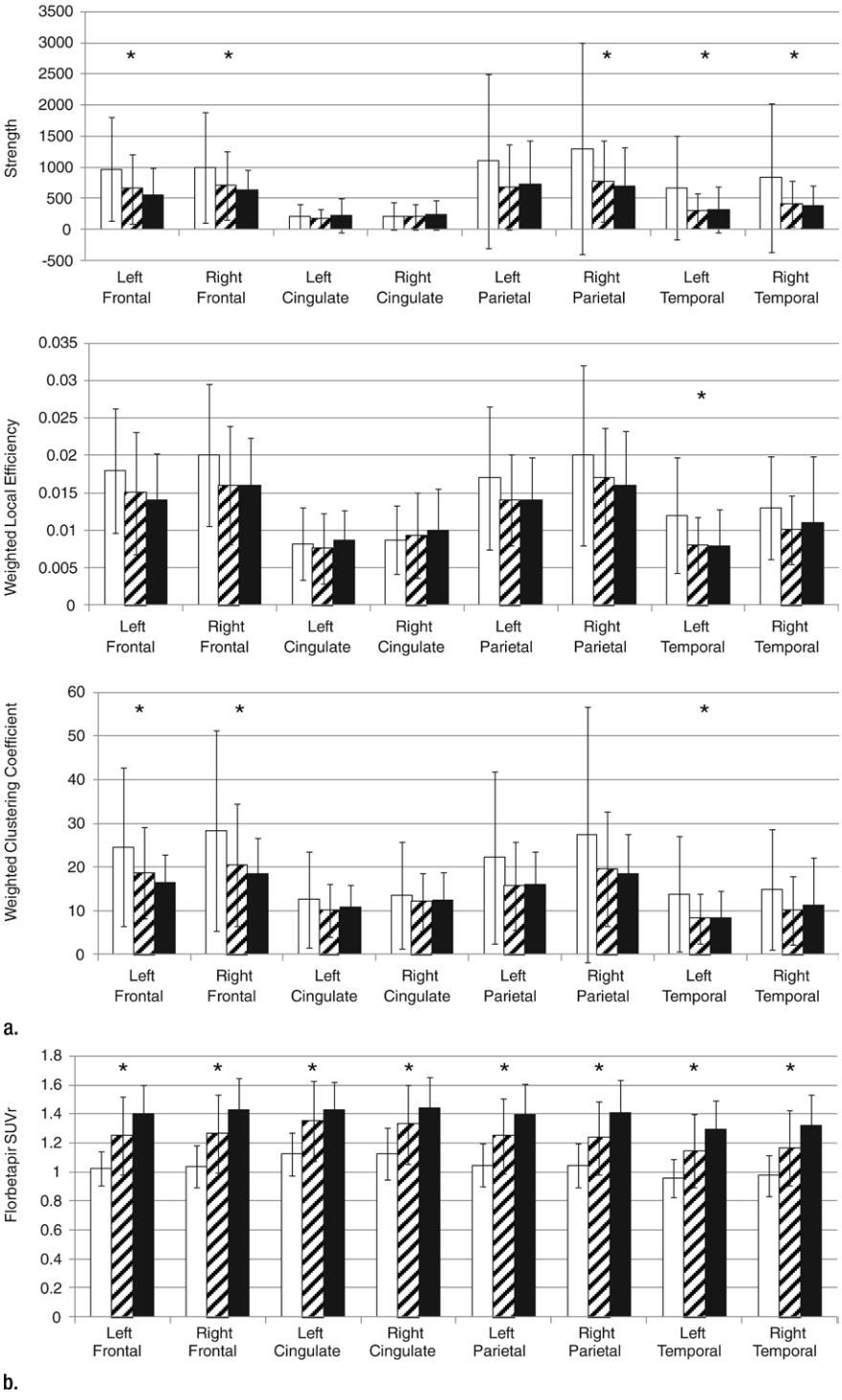

Figure 1: **(a)** Bar plots of weighted network metrics in each composite cortical region, separated by diagnostic group. Bar height represents the mean metric value, and error bar represents one standard deviation from the mean. $* P < .05$ for analysis of variance. **(b)** Bar plots show network metrics for florbetapir SUVr in each composite cortical region, separated by diagnostic group. Bar height represents the mean metric value, and error bar represents one standard deviation from the mean. $* P < .05$ for analysis of variance.

of these demographic variables in our sample. The variable a_i denotes the random effect for patient i, assumed to have a zero mean normal distribution. The variables $\alpha_{MCI,i}$ and $\alpha_{AD,i}$ denote the additional effects of disease in the MCI and AD groups respectively, while $\alpha_{F,i}$ denotes the additional effects of sex in female patients. The variable $\alpha_{R,k}$ denotes the additional effects of region other than left frontal. The coefficient b_p denotes the baseline effect of every additional unit of standardized uptake value in the left frontal region ($SUVr_{LF}$), while the coefficients $b_{p,MCI}$ and $b_{p,AD}$ denote the differential effect of every additional unit of standardized uptake value in the left frontal region for patients with MCI and those with AD. The coefficient $b_{P,k}$ denotes the differential effect of every additional unit of standardized uptake value in region k, other than left frontal. Finally, the terms b_a and b_e denote the effect of every additional unit of age and education. Time between acquisition of DT images and florbetapir PET images was not included in the model.

Note that the model specified in Equation (2) enables simultaneous analysis of data across all brain regions from each patient. The random effect of patient is used to model the resulting correlation in measurements. Joint modeling ensures that the estimates are statistically efficient and that P values do not need to be subsequently corrected for multiple comparisons.

All statistical analyses were implemented by using R software, version 3.0.1 *(www.r-project.org)*. All statistical analyses were performed by two authors (J.W.P., K.R.C.; 5 and 20 years of experience, respectively).

Results

There were 102 patients (64 male, 38 female) in this study: 37 with NC, 44 with

Table 2

Results of Fitting Linear Mixed-Effects Model to Strength Network Connectivity Metric

Model Term	Estimated Effect*	Standard Error	*P* Value
Baseline†	8.29	0.38	<.00001‡
Amyloid SUVr§	−1.55	0.34	.00001‡
MCI group‖	−1.26	0.40	.002‡
AD group‖	−1.05	0.52	.05‡
Age#	−0.02	0.01	.06
Female sex#	−0.20	0.13	.13
Education#	−0.02	0.02	.44
Cortical region**			
Left parietal	−0.09	0.26	.73
Left temporal	−0.73	0.26	.005‡
Right cingulate	−1.47	0.27	<.00001‡
Left cingulate	−1.72	0.27	<.00001‡
Right frontal	0.01	0.25	.97
Right parietal	0.18	0.26	.49
Right temporal	−0.42	0.26	.10
Amyloid SUVr			
MCI group††	1.03	0.34	.003‡
AD group††	0.92	0.41	.02‡
Cortical region‡‡			
Left parietal	0.10	0.21	.65
Left temporal	−0.07	0.22	.76
Right cingulate	0.09	0.21	.68
Left cingulate	0.29	0.21	.18
Right frontal	0.07	0.21	.75
Right parietal	−0.02	0.21	.92
Right temporal	−0.10	0.22	.65

Note.—Refer to Equation 2 for full model definition.

* Effect (either additive or differential) of each row on the network metric value.

† Network metric value in the left frontal region of a 74-year-old man with 16 years of education and a left frontal florbetapir SUVr of 0.

‡ *P* value indicates a significant difference.

§ Differential effect (slope) of each unit of florbetapir SUVr in the left frontal region.

‖ Additive effect of the diagnostic group (MCI or AD).

Additive effects of each of the demographic variables.

** Additive effect of modeling the network metric in a region other than the left frontal region.

†† Interaction effect that modifies the differential effect (slope) of each unit of amyloid SUVr based on the diagnostic group (MCI or AD).

‡‡ Interaction effect that modifies the differential effect (slope) of each unit of amyloid SUVr when modeling the network metric in a region other than the left frontal region.

MCI, and 21 with AD (Table 1). The ages were similar across groups. There were more men than women in each diagnostic group. Patients in the NC group tended to have more years of education than did patients in the MCI or AD group. As expected, the Alzheimer's Disease Assessment Scale-cognitive subscale (or ADAS-cog, a clinical measure of cognitive performance) increased from the NC group to the MCI group to the AD group and corresponded to a decrease in cognitive performance.

Analysis of Structural Connectome Metrics across Diagnostic Groups

The regional average of node degree, strength, local efficiency (weighted and unweighted), and clustering coefficient (weighted and unweighted) and their associations with diagnostic group are shown in Figure 1a. There were significant differences across the diagnostic groups for node degree (left and right parietal regions: $P = .03$ and $P = .003$, respectively), node strength (left frontal, right frontal, right parietal, left temporal, and right temporal regions: $P = .03$, $P = .04$, $P = .04$, $P = .007$, and $P = .03$, respectively), weighted local efficiency (left temporal region: $P = .05$), and weighted clustering coefficient (left frontal, right frontal, and left temporal regions: $P = .04$, $P = .05$, and $P = .02$, respectively). There were no significant differences for unweighted local efficiency or unweighted clustering coefficient.

Analysis of Amyloid Burden across Diagnostic Groups

There was a significant increase in the amyloid burden across the diagnostic groups in all cortical regions, as expected ($P < .001$ for all regions) (Fig 1b). There was no significant difference in florbetapir SUVr between regions among the same diagnostic group.

Analysis of Structural Connectome Metrics and Amyloid Burden

There were significant associations between florbetapir SUVr and each of the weighted connection metrics (strength, $P = .00001$; weighted local efficiency, $P = .00001$; and weighted clustering coefficient, $P = .0006$) (Tables 2–4). For every 0.1-unit increase in florbetapir SUVr, there was a decrease of 14% in strength, 11% in weighted local efficiency, and 9% in weighted clustering coefficient, regardless of the analyzed cortical region or, in the case of weighted local efficiency and clustering coefficient, diagnostic group. There were no significant associations between florbetapir SUVr and any of the unweighted network metrics. There was a significant interaction between florbetapir SUVr and diagnostic group for strength, with the NC group having the greatest effect of SUVr.

Estimated standard deviations for the random effect due to patient were higher than the estimated standard deviations of residuals for all three clustering metrics, suggesting a high degree of interpatient variability (Table

E1 [online]). The distribution of residuals had an approximately normal distribution for all three metrics; this justified use of the log transformation of the response (Figs E1–E3 [online]). There was no strong evidence of heteroscedasticity in the model for any of the metrics (Figs E1–E3 [online]).

Table 3

Results of Fitting Linear Mixed-Effects Model to Weighted Local Efficiency Network Connectivity Metric

Model Term	Estimated Effect	Standard Error	*P* Value
Baseline	−2.97	0.28	<.00001*
Amyloid SUVr	−1.13	0.25	.00001*
MCI group	−0.45	0.30	.13
AD group	−0.32	0.38	.40
Age	−0.01	0.01	.06*
Female sex	0.02	0.10	.82
Education	−0.00	0.02	.86
Cortical region			
Left parietal	−0.26	0.19	.18
Left temporal	−0.64	0.19	.001*
Right cingulate	−0.75	0.19	.0001*
Left cingulate	−0.86	0.20	.00002*
Right frontal	0.11	0.19	.56
Right parietal	−0.03	0.19	.87
Right temporal	−0.50	0.19	.01*
Amyloid SUVr			
MCI group	0.39	0.25	.12
AD group	0.39	0.30	.19
Cortical region			
Left parietal	0.15	0.16	.32
Left temporal	−0.02	0.16	.92
Right cingulate	0.16	0.15	.29
Left cingulate	0.16	0.16	.31
Right frontal	−0.00	0.15	>.99
Right parietal	0.11	0.16	.46
Right temporal	0.04	0.16	.78

Note.—Refer to Table 2 for a description of the meaning of each row.

* *P* value indicates a significant difference.

Discussion

Our results show that increased cortical amyloid deposition, as measured with florbetapir PET, is significantly associated with changes in the topology of the structural connectome, as measured with graph theoretical metrics. Specifically, there were significant inverse associations between florbetapir SUVr and each of the weighted structural connectome metrics: strength, weighted local efficiency, and weighted clustering coefficient. The degree of amyloid burden was an additional and more significant factor associated with decreased network metrics than was diagnostic group, in which the MCI and AD groups showed decreased network metrics when compared with the NC group. Increased amyloid deposition did not affect the metric values of any particular region more than others. This is evidenced by the lack of a significant florbetapir SUVr by region interaction. Most importantly, these results show that large-scale structural network changes can be detected in the presence of amyloid pathology, even in the preclinical stages of AD.

It is interesting to note that the differential effect (slope) of every unit increase of florbetapir SUVr on the strength metric was significantly less in the AD and MCI groups than in the NC group. This is supported by a significant florbetapir SUVr by group interaction for the AD and MCI groups. We speculate that this result suggests that damage to the structural connectome may represent an early event in the pathophysiology of AD, paralleling or closely following amyloid deposition. We hypothesize that increased amyloid burden may be associated with a slower rate of decline in network metrics in the MCI or AD groups because of fewer viable connections to undergo degeneration in symptomatic patients, thus decreasing the effects of accumulating amyloid burden. Indeed, although an increase in amyloid deposition is seen in patients with preclinical AD and those with milder stages of AD, longitudinal biomarker studies have shown that degenerative changes and cognitive decline accelerate in patients with moderate stages of AD (2,25,26).

We also showed significant differences in multiple measures of the structural connectome among patients with NC, patients with MCI, and patients with AD. Interestingly, the weighted versions of the structural connectome metrics had the most significant differences across diagnostic group, suggesting that information on the number of diffusion streamlines carries critical information related to amyloid burden. It should be noted that the variability of some of the weighted metrics is high, particularly the strength metric in the bilateral parietal and temporal lobes. This may be due to inherent patient-level differences in the structural connectome manifested by the tractographic reconstruction algorithm. The inclusion of a patient-level random effect in the linear mixed-effects statistical model, as was used in this study, is one method of adjusting for possible inherent patient-level differences across all regions analyzed. The relatively large standard deviation of this random effect suggests that this is an important term for all three metrics analyzed in this study.

Table 4

Results of Fitting Linear Mixed-Effects Model to Weighted Clustering Coefficient Network Connectivity Metric

Model Term	Estimated Effect	Standard Error	*P* Value
Baseline	4.05	0.29	<.00001*
Amyloid SUVr	−0.92	0.27	.0006*
MCI group	−0.65	0.31	.04*
AD group	−0.19	0.41	.63
Age	−0.01	0.01	.29
Female sex	−0.17	0.10	.10
Education	−0.01	0.02	.77
Cortical region			
Left parietal	−0.39	0.20	.06
Left temporal	−0.78	0.20	.0001*
Right cingulate	−0.59	0.21	.005*
Left cingulate	−0.68	0.21	.001*
Right frontal	0.17	0.20	.39
Right parietal	−0.16	0.20	.45
Right temporal	−0.70	0.20	.0005*
Amyloid SUVr			
MCI group	0.50	0.27	.06
AD group	0.21	0.32	.52
Cortical region			
Left parietal	0.20	0.17	.23
Left temporal	−0.06	0.17	.74
Right cingulate	0.08	0.16	.61
Left cingulate	0.07	0.17	.68
Right frontal	−0.06	0.16	.72
Right parietal	0.16	0.17	.34
Right temporal	0.05	0.17	.78

Note.—Refer to Table 2 for a description of the meaning of each row.

* *P* value indicates a significant difference.

Interestingly, visual inspection of connectome maps revealed no discernible systematic differences among groups in the nodal connections, suggesting that structural connectome metrics are critical in this regard (Fig 2).

Previous studies in which researchers examined the functional connectome with functional MR imaging have shown the strongest group- and amyloid-related effects in the posterior cingulate regions (11–13,27). In these studies, functional connectivity refers to correlations of time series between regions, that is, dynamic coupling. Loss of coupling of time-dependent neuronal activity can be driven by disruption of direct neural connections or by some other cause, such as loss of connections to a common driver, decoupling driven by abnormal changes involving one or both regions, or remodeling elsewhere in the network. Our analysis was not designed to determine which structural connections might be involved in the loss of dynamic coupling in functional analyses. Such connections could be both long- and short-ranged because the posterior cingulate region is highly connected both locally (to the precuneus and retrosplenial cortex) and globally (particularly to the medial temporal lobe but also to the frontal and parietal regions). Further analyses focusing on specific connections may help elucidate important links between structure and function.

The main limitations of this study are its cross-sectional nature and the relatively small sample. We focused on four brain regions highly affected by β-amyloid that previously have been shown to have high test-retest reliability in quantitative analysis of the florbetapir PET images. Hence, our correlations were driven by only these regions. Specifically, the analyzed regions did not include the inferior temporal cortex, entorhinal cortex, amygdalae, or hippocampi, which are areas known to be affected early in the course of AD. Also, while comparison of DT imaging tractography with histologic tractography has shown good visual agreement between collections of DT imaging streamlines and histologic fiber tracts (28,29), to our knowledge, there is no quantitative validation that the number of streamlines has any direct physiologic meaning (30). The number of streamlines is instead dependent on the parameters used in the construction of the streamlines themselves. DT imaging tractography was performed by using a standardized protocol for all patients. Thus, within this analysis, the number of streamlines can be reasonably taken to have consistent meaning between patients. Finally, no atrophy correction was undertaken in this study. It is reasonable to assume that, in the setting of brain atrophy, the strength metric might decrease. However, the largest effect of amyloid on the strength metric in our statistical model was in patients with NC, who would not be expected to have measurable cortical atrophy. Also, it is not apparent if atrophy would preferentially affect particular cortical connections, thereby changing the complexity of the structural connectome and consequent measures, such as local efficiency and clustering coefficient.

In summary, our cross-sectional study of baseline data from a national cohort of patients with AD, MCI, or NC shows that increased cortical amyloid deposition is significantly associated with alterations in the topology of the structural connectome. The prominence of these changes in patients with NC raises the possibility that damage to the

Figure 2

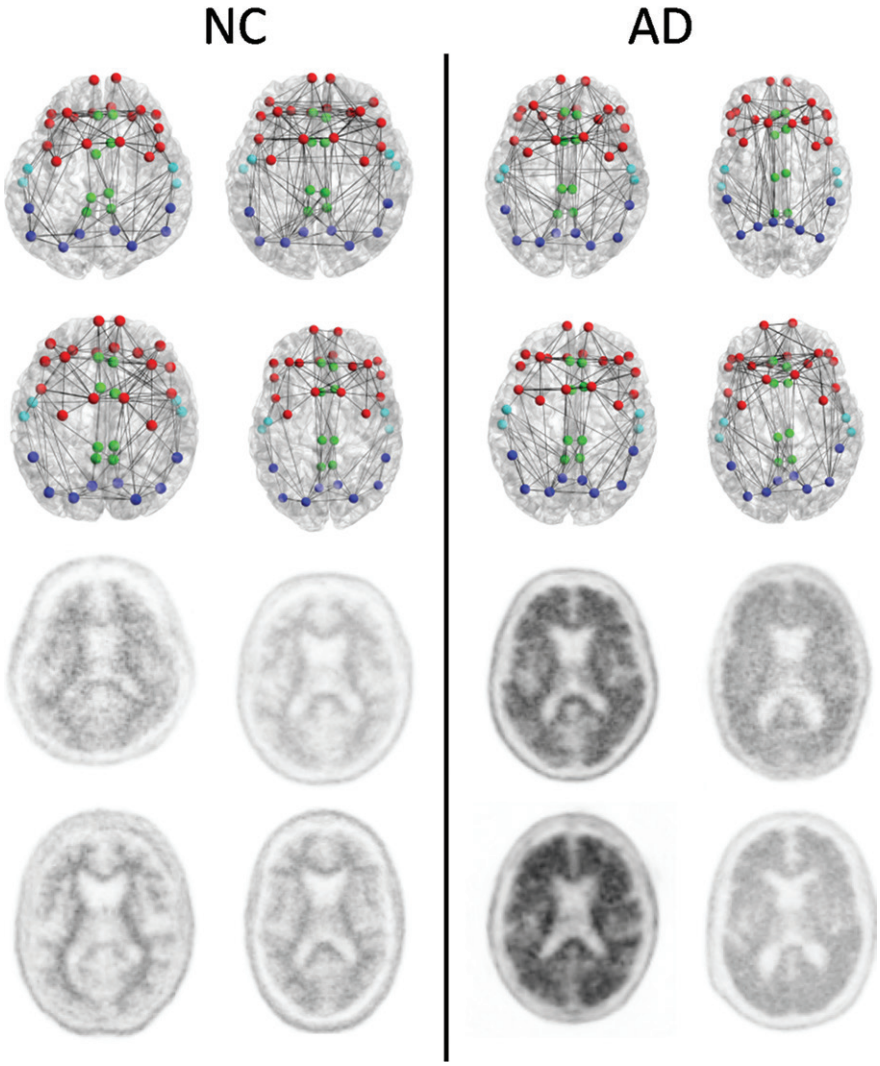

Figure 2: Structural connectomes (top two rows) and corresponding florbetapir PET images (bottom two rows) in the four patients with NC with the lowest whole cortex amyloid burden (left) and the four patients with AD with the highest whole cortex amyloid burden (right) focused on the composite regions used in connectome versus amyloid analysis. Nodes represent the centroids of the FreeSurfer parcellations in the frontal (red), cingulate (green), temporal (light blue), and parietal (dark blue) regions. Edges (lines) are weighted by the number of streamlines between two nodes; the thicker the edge, the greater the number of streamlines. Note that differences in edge widths and organization are not easily discernible between patients with AD and those with NC. The figures were generated with the BrainNet Viewer *(http://www.nitrc.org/projects/bnv/)*. This is merely a schematic intended to show the concepts and is not intended to show any visually discernible generalizable difference between the patients with NC and those with AD. Structural network metrics provide more sensitive information about the connectome than are apparent through visualization alone.

structural connectome may occur at a preclinical stage in patients at risk. Longitudinal clinical and imaging data from future studies will be needed to confirm these findings and determine their diagnostic and prognostic importance.

Acknowledgments: Data used in preparation of this article were obtained from the ADNI database *(adni.loni.ucla.edu)*. As such, the ADNI investigators contributed to the design and implementation of ADNI and/or provided data but did not participate in analysis or writing of this report. A complete listing of ADNI investigators can be found at *http://adni.loni.ucla.edu/wp-content/uploads/how_to_apply/ADNI_Acknowledgement_List.pdf*. The authors thank Tim Turkington, PhD, for useful discussions on the processing of PET data. One author (C.L.) is supported in part by NIH R01MH096979. Data collection and sharing for this project were funded by the ADNI. ADNI is funded by the National Institute on Aging, the National Institute of Biomedical Imaging and Bioengineering, and through generous contributions from the following: Alzheimer's Association; Alzheimer's Drug Discovery Foundation; BioClinica.; Biogen Idec; Bristol-Myers Squibb; Eisai; Elan Pharmaceuticals.; Eli Lilly; F. Hoffmann-La Roche and its affiliate, Genentech; GE Healthcare; Innogenetics; IXICO; Janssen Alzheimer Immunotherapy Research & Development.; Johnson & Johnson Pharmaceutical Research & Development; Medpace; Merck; Meso Scale Diagnostics; NeuroRx Research; Novartis Pharmaceuticals; Pfizer; Piramal Imaging; Servier; Synarc; and Takeda Pharmaceutical Company. The Canadian Institutes of Health Research is providing funds to support ADNI clinical sites in Canada. Private sector contributions are facilitated by the Foundation for the National Institutes of Health *(www.fnih.org)*. The grantee organization is the Northern California Institute for Research and Education, and the study is coordinated by the Alzheimer's Disease Cooperative Study at the University of California, San Diego. ADNI data are disseminated by the Laboratory for Neuroimaging at the University of California, Los Angeles.

Disclosures of Conflicts of Interest: J.W.P. No relevant conflicts of interest to disclose. **A.G.** No relevant conflicts of interest to disclose. **P.M.D.** Financial activities related to the present article: none to disclose. Financial activities not related to the present article: is a consultant to Avid/Lilly, Accera, AstraZeneca, Genomind, Baxter, Abbvie, TauRx, Cognoptix, Piramal, Sonexa, Lundbeck/Takeda, Targacept, Danone, Neurocog Trials, and EnVivo; institution received grants from Elan, Avid/Lilly, Novartis, Janssen, Pfizer/Medivation, and Neuronetrix; gave lectures for Lundbeck; receives royalties for St Martin's Press; developed educational presentations for Postgraduate Press; owns stock in Sonexa, Clarimedix, Adverse Events, and Maxwell; received compensation for meeting expenses from Biogen X-prize. Other relationships: none to disclose. **K.R.C.** No relevant conflicts of interest to disclose. **C.L.** No relevant conflicts of interest to disclose. **J.R.P.** Financial activities related to the present article: none to disclose. Financial activities not related to the present article: is on the speaker's bureau of Quintiles, is on the advisory board of Janssen Alzheimer Immunotherapy and Piramel. Other relationships: none to disclose.

References

1. Petrella JR. Neuroimaging and the search for a cure for Alzheimer disease. Radiology 2013;269(3):671–691.

2. Jack CR Jr, Knopman DS, Jagust WJ, et al. Tracking pathophysiological processes in Alzheimer's disease: an updated hypothetical model of dynamic biomarkers. Lancet Neurol 2013;12(2):207–216.

3. Delbeuck X, Van der Linden M, Collette F. Alzheimer's disease as a disconnection syndrome? Neuropsychol Rev 2003;13(2):79–92.

4. Clark CM, Schneider JA, Bedell BJ, et al. Use of florbetapir-PET for imaging beta-amyloid pathology. JAMA 2011;305(3):275–283.

5. Doraiswamy PM, Sperling RA, Coleman RE, et al. Amyloid-β assessed by florbetapir F 18 PET and 18-month cognitive decline: a multicenter study. Neurology 2012;79(16):1636–1644.

6. Sporns O. The human connectome: origins and challenges. Neuroimage 2013;80:53–61.

7. Bullmore E, Sporns O. Complex brain networks: graph theoretical analysis of structural and functional systems. Nat Rev Neurosci 2009;10(3):186–198.

8. Rubinov M, Sporns O. Complex network measures of brain connectivity: uses and interpretations. Neuroimage 2010;52(3):1059–1069.

9. Buckner RL, Snyder AZ, Shannon BJ, et al. Molecular, structural, and functional characterization of Alzheimer's disease: evidence for a relationship between default activity, amyloid, and memory. J Neurosci 2005;25(34):7709–7717.

10. Greicius MD, Srivastava G, Reiss AL, Menon V. Default-mode network activity distinguishes Alzheimer's disease from healthy aging: evidence from functional MRI. Proc Natl Acad Sci U S A 2004;101(13):4637–4642.

11. Hedden T, Van Dijk KR, Becker JA, et al. Disruption of functional connectivity in clinically normal older adults harboring amyloid burden. J Neurosci 2009;29(40):12686–12694.

12. Petrella JR, Sheldon FC, Prince SE, Calhoun VD, Doraiswamy PM. Default mode network connectivity in stable vs progressive mild cognitive impairment. Neurology 2011;76(6):511–517.

13. Sperling RA, Laviolette PS, O'Keefe K, et al. Amyloid deposition is associated with impaired default network function in older persons without dementia. Neuron 2009;63(2):178–188.

14. Lo CY, Wang PN, Chou KH, Wang J, He Y, Lin CP. Diffusion tensor tractography reveals abnormal topological organization in structural cortical networks in Alzheimer's disease. J Neurosci 2010;30(50):16876–16885.

15. Bai F, Shu N, Yuan Y, et al. Topologically convergent and divergent structural connectivity patterns between patients with remitted geriatric depression and amnestic mild cognitive impairment. J Neurosci 2012;32(12):4307–4318.

16. Shu N, Liang Y, Li H, et al. Disrupted topological organization in white matter structural networks in amnestic mild cognitive impairment: relationship to subtype. Radiology 2012;265(2):518–527.

17. Reijmer YD, Leemans A, Caeyenberghs K, et al. Disruption of cerebral networks and cognitive impairment in Alzheimer disease. Neurology 2013;80(15):1370–1377.

18. Landau SM, Mintun MA, Joshi AD, et al. Amyloid deposition, hypometabolism, and longitudinal cognitive decline. Ann Neurol 2012;72(4):578–586.

19. Fischl B, Salat DH, Busa E, et al. Whole brain segmentation: automated labeling of neuroanatomical structures in the human brain. Neuron 2002;33(3):341–355.

20. Hostage CA, Roy Choudhury K, Doraiswamy PM, Petrella JR; Alzheimer's Disease Neuroimaging Initiative. Dissecting the gene dose-effects of the APOE ε4 and ε2 alleles on hippocampal volumes in aging and Alzheimer's disease. PLoS ONE 2013;8(2):e54483.

21. Joshi AD, Pontecorvo MJ, Clark CM, et al. Performance characteristics of amyloid PET with florbetapir F 18 in patients with alzheimer's disease and cognitively normal subjects. J Nucl Med 2012;53(3):378–384.

22. Daducci A, Gerhard S, Griffa A, et al. The connectome mapper: an open-source processing pipeline to map connectomes with MRI. PLoS ONE 2012;7(12):e48121.

23. Jenkinson M, Bannister P, Brady M, Smith S. Improved optimization for the robust and accurate linear registration and motion correction of brain images. Neuroimage 2002;17(2):825–841.

24. Bassett DS, Bullmore E. Small-world brain networks. Neuroscientist 2006;12(6):512–523.

25. Castellani RJ, Lee HG, Siedlak SL, et al. Reexamining Alzheimer's disease: evidence for a protective role for amyloid-beta protein precursor and amyloid-beta. J Alzheimers Dis 2009;18(2):447–452.

26. Lee HG, Casadesus G, Zhu X, Takeda A, Perry G, Smith MA. Challenging the amyloid cascade hypothesis: senile plaques and amyloid-beta as protective adaptations to Alzheimer disease. Ann N Y Acad Sci 2004;1019:1–4.

27. Petrella JR, Wang L, Krishnan S, et al. Cortical deactivation in mild cognitive impairment: high-field-strength functional MR imaging. Radiology 2007;245(1):224–235. [Published correction appears in Radiology 2008;246(1):338.]

28. Dyrby TB, Søgaard LV, Parker GJ, et al. Validation of in vitro probabilistic tractography. Neuroimage 2007;37(4):1267–1277.

29. Dauguet J, Peled S, Berezovskii V, et al. Comparison of fiber tracts derived from in-vivo DTI tractography with 3D histological neural tract tracer reconstruction on a macaque brain. Neuroimage 2007;37(2):530–538.

30. Fornito A, Zalesky A, Breakspear M. Graph analysis of the human connectome: promise, progress, and pitfalls. Neuroimage 2013;80:426–444.